

Study on Response Time Hysteresis Model of Smoke Detectors in Aircraft Cargo Compartment

Hongwei Cui ^{1,2}, Chenran Ruan ¹, Shengdong Wang ², Song Lu ^{1,*} , Heping Zhang ¹ and Minqiang Wang ²

¹ State Key Laboratory of Fire Science, University of Science and Technology of China, Hefei 230026, China; cuihongwei666@mail.ustc.edu.cn (H.C.); ruanchenran@mail.ustc.edu.cn (C.R.); zhanghp@ustc.edu.cn (H.Z.)

² Tianjin Aviation Electro-Mechanical Co., Ltd., Tianjin 300381, China; wangsd012@avic.com (S.W.); wangmq006@avic.com (M.W.)

* Correspondence: lusong@ustc.edu.cn

Abstract: A fire in the cargo compartment has a major impact on civil aviation flight safety, and according to the airworthiness clause of the CCAR-25, the detector must sound an alarm within 1 min of a fire in the cargo compartment. As for the cargo compartment of large transport aircrafts, the internal space is high and open, and the smoke movement speed becomes slower with significant cooling in the process of diffusion. Hysteresis can occur in smoke detectors because of their internal labyrinth structure, which causes the detector's internal and external response signals to be out of sync. This research employs a numerical simulation to examine the detector response parameters under an ambient wind speed of 0.1–0.2 m/s and fits a Cleary two-stage hysteresis model, where $\tau_1 = 0.09u^{-1.43}$ and $\tau_2 = 0.67u^{-1.59}$. Finally, multiple full-scale cargo cabin experiments were conducted to validate the prediction model. The results show that the model's predicted alarm range is 43.1 s to 49.0 s, and the actual alarm time obtained by the experiment falls within this interval, confirming the model's accuracy and providing theoretical support for the structural design and layout of the aircraft cargo cabin smoke detector.

Keywords: aircraft cargo; smoke detector; civil aircraft; time lag; numerical simulation; system design



Citation: Cui, H.; Ruan, C.; Wang, S.; Lu, S.; Zhang, H.; Wang, M. Study on Response Time Hysteresis Model of Smoke Detectors in Aircraft Cargo Compartment. *Fire* **2024**, *7*, 317. <https://doi.org/10.3390/fire7090317>

Academic Editor: Kaihua Lu

Received: 5 July 2024

Revised: 8 September 2024

Accepted: 9 September 2024

Published: 13 September 2024



Copyright: © 2024 by the authors. Licensee MDPI, Basel, Switzerland. This article is an open access article distributed under the terms and conditions of the Creative Commons Attribution (CC BY) license (<https://creativecommons.org/licenses/by/4.0/>).

1. Introduction

According to Article 25.858 of the Civil Aviation Regulations of the People's Republic of China, the cargo compartment smoke detection system shall give visual instructions to the flight crew within one minute of the fire, and according to the AS8036 "Cargo Compartment Fire Detection Device" and HB7098-1994 [1] "Minimum Performance Requirements for Smoke Detectors in the Cargo Compartment and Baggage Compartment of Civil Aircraft" standards, photoelectric smoke detectors should output an alarm signal within thirty seconds after the air sample enters the detector. It can be inferred that the smoke detector response time is likely to account for a significant portion of the overall response time of the smoke detection system. The response of the smoke detector is heavily influenced by its own structure, as when smoke reaches the outside of the detector, it takes some time to enter the labyrinth inside the detector and reach the alarm concentration before the alarm, which is known as the lag time, and if the structure of the smoke detector is not reasonably designed, it is difficult to ensure that the alarm sounds within 1 min. At the moment, the response time of the smoke detector is mainly determined through the experimental test method. As there is a lack of a positive design in the theoretical analysis process, if the test process does not pass, it is necessary to re-design until it meets current standards, which is time-consuming and laborious. As a result, the investigation of the hysteresis effect of smoke detector responses for the design and selection of aircraft cargo hold smoke detectors has both engineering and scientific significance [2].

Previous researchers conducted numerous experimental and simulation studies to improve the fire detection capability of aircraft cargo compartments, including the scattering

characteristics of smoke and temperature distribution inside cargo compartments when a fire occurs, as well as the response characteristics of detectors. Some researchers have concentrated on analyzing the thermal properties of cabin combustibles in order to provide theoretical guidelines for the design and layout of detectors based on the smoke and temperature-change characteristics of fire. Wang Jie et al. [3] carried out fire experiments in a simulated Boeing forward cargo hold to investigate the ceiling smoke and temperature distribution of an early fire. Li Cong et al. [4] investigated the combustion characteristics of full-size cabin fires with different ignition source locations. Keller et al. [5] studied the optical properties of standard EN54 test fires, and the results showed that there was no significant difference in the particle size distribution of smoldering/pyrolysis or open fire smoke. Kruell et al. [6] proposed a new method for testing the sensitivity of smoke detectors to false alarms caused by interfering aerosols such as water vapor and dust. However, conducting a comprehensive aircraft cargo experiment is often time-consuming and labor-intensive. Therefore, with the rapid improvement of computational performance, some scholars use numerical simulation technology to study aircraft cargo compartment fires. A computational model for predicting smoke and gas transport in aircraft cargo compartments has been validated for use in the certification process of cargo compartment fire detection systems. Zhou Yaozhi [7] and Zheng Rong et al. [8] investigated the scattering characteristics of open-flame cloudy combustion smoke and dust, as well as the other interference sources of various common materials in aircraft cargo compartments, through numerical calculations. Chen Xiyuan [9,10] and Papa et al. [11] established a CFD model of fire smoke dispersion in aircraft cargo compartments and compared the simulation results with the experimental data of the Federal Aviation Administration Kaiyuan, which verified the accuracy of the model. Blake et al. [12] developed a computer code for transient computational fluid dynamics for predicting the transport of smoke, heat and gas species in the cargo hold, which can be used to identify the worst-case position of the fire, the optimal position of the detector sensor in the cargo hold, and the sensor alarm level and algorithm required to achieve detection within the required time. The accuracy of the model was verified by real cargo hold experiments. Ezgi et al. [13,14] used the large eddy current simulation turbulence model in FDS software (V6.7.4) to simulate the smoke diffusion of Boeing 707 and DC-10 cargo tanks under different fire scenarios, and the simulation results are in good agreement with the experimental data. Suo et al. [15] constructed a fire prediction model for an aircraft cargo compartment. By changing the location of the fire source, the size of the compartment and the ventilation, the simulation and experimental results under different fire scenarios were compared, and the results show that the model has high reliability and can assist in the design of an optimal detection system for the cargo hold. Lu et al. [16] simulated the changes of smoke, temperature and carbon monoxide concentration in DC-10 cargo compartment fires under different ventilation conditions. Zhang Pei et al. [17] proposed a set of smoke detection system layout methods for aircraft cargo compartments, developed a set of smoke detection system layout optimization platforms based on FDS simulation software and put forward the idea that the characteristic parameters of the smoke detector in the optimized platform can be determined by detailed modeling of the internal structures of smoke detectors.

Due to the complex internal connectivity of the cargo compartment of large transport aircraft and special environmental conditions, such as temperature distribution and ventilation, predicting the development path of smoke in the early stages of a fire will be challenging. Previous studies on aircraft cargo compartment fire simulations mainly focused on simulating and studying the motion law of smoke flow, obtaining the spatial and temporal distributions of a series of fire thermal parameters and then carrying out the evaluation and design of the rationality of the layout of the detection system. This leads to the separation of the fire scene and the detection system, especially the separation from the detector, without considering the interactions between the ambient smoke and the detector. In this paper, the smoke detector and the smoke flow are fused, and a method of calibrating the response time by simulation is proposed for the smoke detector product

under the condition of smoke flow space. Based on the simplified structure of a specific type of smoke detector, this paper will consider the spatiotemporal distribution of smoke characteristic parameters, study the process of smoke entering the detector and predict the smoke detector's response signal through a numerical simulation, in order to provide more complete parameter information for the evaluation and design of aircraft smoke detection systems. This method saves time and money when compared to the most generally used test method in the industrial sector.

2. Hysteresis of Smoke Detectors

2.1. Hysteresis Effect

Photoelectric smoke detectors are typically furnished with a maze, as depicted in Figure 1, which must meet the following functional requirements: (a) protection of working elements within the labyrinth; (b) reduction in velocity of smoke flow in the labyrinth; (c) shading; and (d) prevention of insects and large dust particles from entering. In order to meet these functional requirements, the geometric configuration of the maze is often equipped with insect nets and labyrinth passages. The smoke chamber diameter of the detector selected in this paper is 53.4 mm and the height is 14.5 mm.

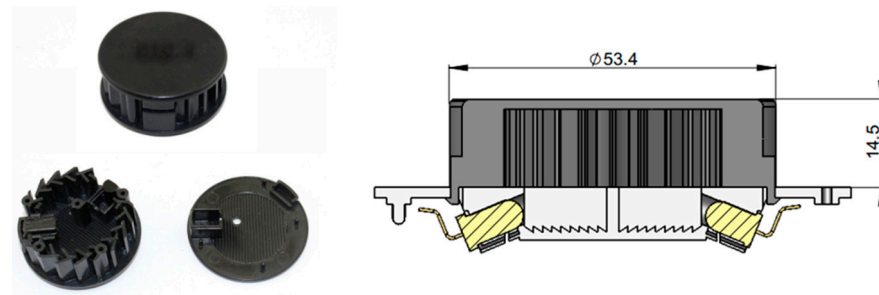


Figure 1. The object and the profile of the maze of the photoelectric smoke detector.

To a certain extent, these settings will result in an obstruction of the flow of smoke into it, and it will behave like a permeable container. For a given detector response threshold, as shown in Figure 2, a hysteresis effect will occur due to the desynchronization of the response signals in the maze and outside the maze $\Delta t = t_B - t_A$. A smoke detector 'hysteresis effect' is a detector response to the basic characteristics of the fire after the occurrence of the smoke generation process, smoke transport process and the role of the smoke and detector process, where each process has a relevant theoretical model. Among them, the actions of the smoke and detector are the main reasons for the hysteresis time, while the labyrinth structure of the detector and the anti-insect net will directly affect the hysteresis time of the detector.

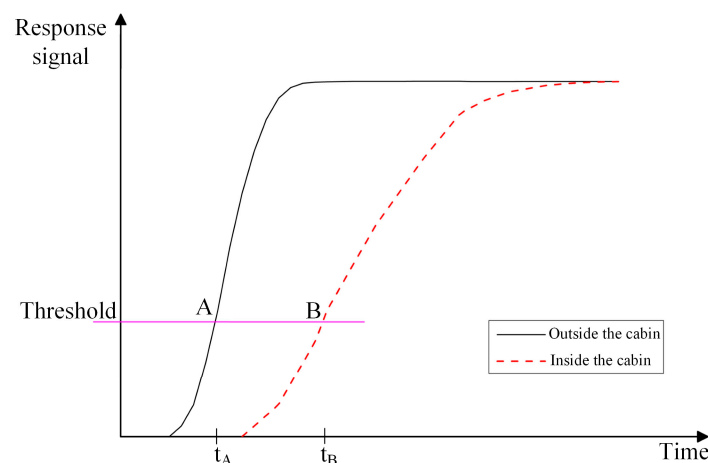


Figure 2. Response hysteresis of smoke detector.

2.2. Hysteresis Model

As mentioned in the previous section, for a given detector response threshold, a hysteresis effect will occur due to the non-synchronization of the response signals in the maze and outside the maze $\Delta t = t_B - t_A$. If the smoke concentration outside the maze is $\rho(t)$ at a certain time, and the smoke mass concentration is $\tilde{\rho}(t)$ inside the maze, then the difference between the inside and outside of the detector is $\rho(t) - \tilde{\rho}(t)$. The experimental research of the scholar Heskestad [18] believes that after time τ , the mass concentration in the labyrinth reaches $\rho(t)$, that is, $\rho(t) = \tilde{\rho}(t + \tau)$, where τ is inversely proportional to the smoke flow velocity u in front of the detector at time t , which is written as $\tau = L \cdot u^{-1}$, L is a coefficient with a length dimension, Heskestad calls it the characteristic length, which represents the distance that the imaginary smoke flow outside the maze needs to pass through the labyrinth.

$$\begin{cases} \frac{\partial \tilde{\rho}(t)}{\partial t} = \frac{\rho(t) - \tilde{\rho}(t)}{\tau} \\ \tau = L \cdot u^{-1} \end{cases} \quad (1)$$

Brozovsky [19] proposed the concept of “critical velocity” for the hysteresis effect of the detector, and he believed that once the smoke flow velocity at the front end of the detector is below this critical velocity u_0 , the hysteresis time increases exponentially with the decrease in velocity, and even if the optical density of the surrounding environment is much higher than the UL standard [20], the detector cannot respond effectively, and the detector can be considered to fail at this time. Based on this concept, the Heskestad model was modified to $\tau = L \cdot (u - u_0)^{-1} (u > u_0)$. In his experiment, after the test wind speed was less than 0.16 m/s, the hysteresis of the detector increased sharply and was close to the failure state.

Cleary’s [21] experimental results show that the Heskestad model is in good agreement with fast smoke flow, but for slow smoke flow, only the characteristic length L parameter cannot be effectively agreed with a large number of experimental data, and he found that the hysteresis time τ is not simply inversely proportional to the first square of u . Based on the above problems, he proposed a two-stage model.

The model describes the hysteresis effect with two parameters with a time dimension, τ_1 and τ_2 , called the residence time and mixing time, respectively. The intramaze response to the extramaze concentrations can be seen as two mixing processes. The concentration of smoke outside the maze can be mixed with the original concentration in the maze after the residence time τ_1 , and the mixing time is τ_2 .

According to Cleary, τ_1 and τ_2 are not simply inversely proportional to the first square of velocity, but can be expressed as follows:

$$\tau_1 = L \cdot u^{-1} \approx a_1 u^{-b_1} \quad (2)$$

$$\tau_2 = L' \cdot u^{-1} \approx a_2 u^{-b_2} \quad (3)$$

where the parameters a_1, a_2, b_1, b_2 take values based on different detectors and different experimental conditions. In summary, the Cleary model describes the following equation:

$$\frac{\partial \tilde{\rho}_{YS}(t)}{\partial t} = \frac{\rho_{YS}(t - \tau_1) - \tilde{\rho}_{YS}(t)}{\tau_2} \quad (4)$$

2.3. Calibration Process of Model Parameters

As shown in Figure 3, the specific steps of calibration parameters can be summarized as follows:

- (a) The stationary segment of the $u(t)$ curve can be calculated as the average value of the time, and u can be calibrated.
- (b) Let t_0 and \tilde{t}_0 be the jumping times of FDS simulation curves of $\rho(t)$ and $\tilde{\rho}(t)$, respectively, and calibrate them according to $\tau_1 = \tilde{t}_0 - t_0$.

- (c) Equation (1) is written as Euler iterative formula 4, the initial value τ_2 is taken, and $\rho(t)$, τ_1 , and τ_2 are calculated according to the $\tilde{\rho}(t)$ obtained by Equation (4).

$$\left\{ \begin{array}{l} \tilde{\rho}(t + \delta t) = \frac{\rho(t-f_1) - \tilde{\rho}(t)}{f_2} \delta t + \tilde{\rho}(t) , t > t_0 + f_1 \\ \tilde{\rho} = 0 \qquad \qquad \qquad t \leq t_0 + f_1 \end{array} \right. \quad (5)$$

- (d) Use the dichotomy to adjust τ_2 so that the calculated curve of $\tilde{\rho}(t)$ is in good agreement with the FDS simulation curve, and τ_2 can be calibrated.
- (e) By changing the air velocity of the tuyere, multiple groups (u , τ_1 and τ_2) values in the wind speed section can be obtained, and then the fitting of $\tau_1 = a_1 u^{-b_1}$ and $\tau_2 = a_2 u^{-b_2}$ can be carried out to determine the characteristic parameters of the detector hysteresis model.

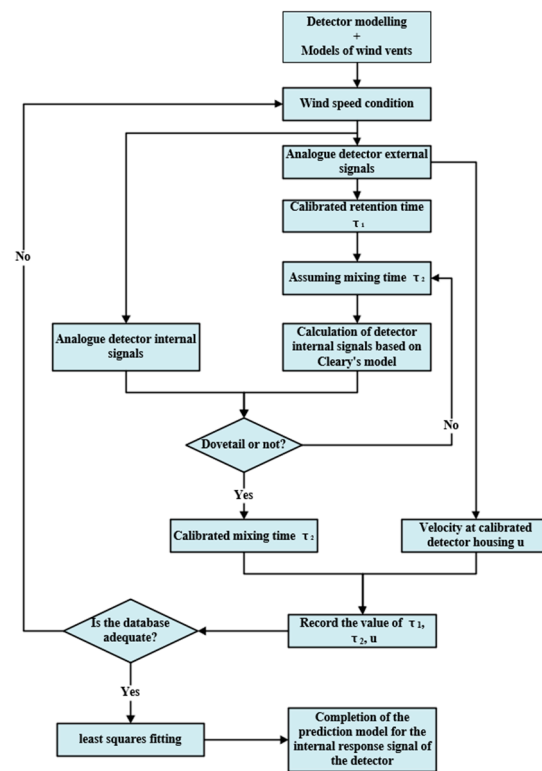


Figure 3. Flowchart for parameter calibration and two-stage hysteresis modelling.

3. Calculation of the Parameters of the Response Time Hysteresis Model for Smoke Detector

3.1. Simulation Model

When using simulation to calibrate the parameters, a reasonable model should be established first, that is, when under different tuyere velocity conditions, the effective velocity $u(t)$ of the roof jet at the outer measurement point of the detector can be ensured. As shown in Figure 4, the spatial dimensions of the model established are $X \times Y \times Z = 1000 \text{ mm} \times 400 \text{ mm} \times 400 \text{ mm}$. The simulation model is divided into two layers, separated by an L-shaped partition, and the left end is connected. The top-right surface pair has an open border, while the bottom-right surface serves as the air entrance. The rest of the surface is closed. The ignition source is located on the lower level near the tuyere, and the reactant is polyurethane. The detector model is built on the higher layer, near the ceiling.

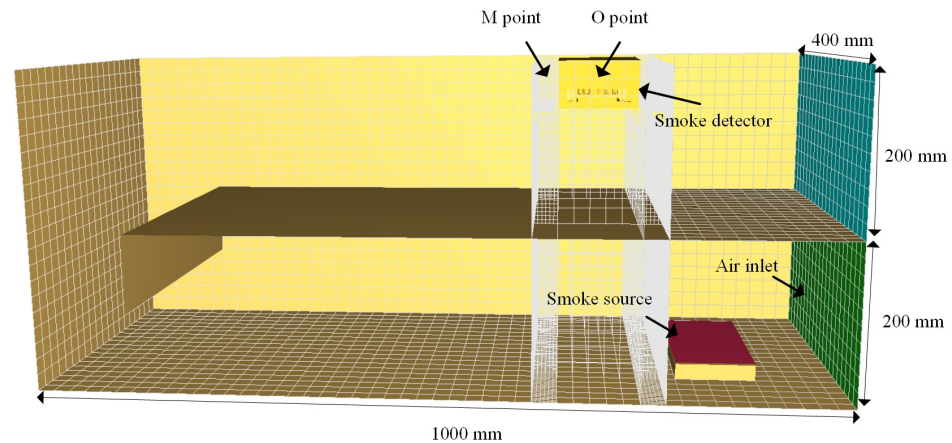


Figure 4. Internal and external measuring points of detector.

We defined a very large smoke soot generation fraction of 0.49 and a very small HRR ignition source of 0.5 kW, which acts as a smoke source to provide smoke in the wind tunnel. Driven by the air flow of the tuyere, the smoke diffuses from right to left in the lower layer, and the existence of the L-shaped partition makes the smoke and the air flow mix well. The smoke flow reaches the left end and rises to the upper layer, showing the characteristics of roof jet flow from left to right, and finally passively diffuses out of the computational domain from the right end of the upper layer.

As shown in Figure 5, the measurement point O and the external measurement point M are selected in the maze of a certain type of smoke detector. Because the heat release rate (HRR) of the ignition source is very small, the smoke flow velocity at the M point outside the detector is only affected by the air flow velocity of the tuyere to a large extent, so a relatively stable u_x and a significantly smaller u_y can be obtained at the M point. Thus, the effective velocity of point M is $u(t) = \sqrt{u_x^2 + u_y^2} \approx u_x(t)$. Outside of the detector, the smoke source factor is taken into account, and the characteristic diameter of the smoke source is as follows: $D^* = \left(\frac{Q}{\rho C_p T \sqrt{g}}\right)^{2/5}$, where C_p is the specific heat of the air, g is the gravitational acceleration, ρ is the atmospheric density and T is the ambient temperature. When the maximum heat release rate of the standard smoke source is 0.5 kW, the characteristic diameter of the smoke source is 43.8 mm, according to the formula, and the minimum grid size should be not less than 0.1 times the characteristic diameter of the smoke source, i.e., 4.38 mm. As the focus area of interest in the simulation calculation is inside the detector, the grid size inside the detector chamber is the smallest, and the grid size of the detector and the periphery, as well as the rest of the space, is gradually increasing, and a total of four sets of grids have been divided in accordance with this criterion as shown in Table 1 (mesh1~4 are getting denser and denser). The smoke concentration inside the detector maze was simulated and calculated, and the results are shown in Figure 6. According to the calculation results, it can be seen that, from mesh1 to mesh3, as the grid becomes denser, the simulated smoke concentration inside the detector labyrinth also gradually increases. As the results gap in the mesh3 and mesh4 calculations is smaller, it can be assumed that the density of the grid in mesh3 has been able to satisfy the requirements of the calculation of the accuracy of mesh3. In order to improve the efficiency of the calculation, we finally chose mesh3 for the simulation. The mesh model was constructed in this way that not only satisfies the calculation accuracy, but also does not lead to calculation overflow. Figure 5 depicts the locations of the monitoring points within the maze.

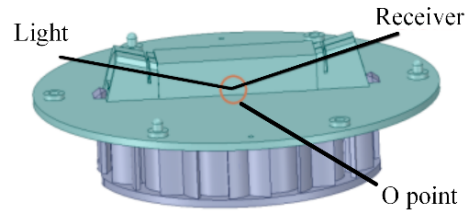


Figure 5. Position of point O inside of smoke labyrinth.

Table 1. Four sets of mesh size.

Grid Size	Inside the Detector	Detector and Surrounding	The Rest of the Space
Mesh1	2	10	40
Mesh2	1.5	7	30
Mesh3	1	5	20
Mesh4	0.5	3	10

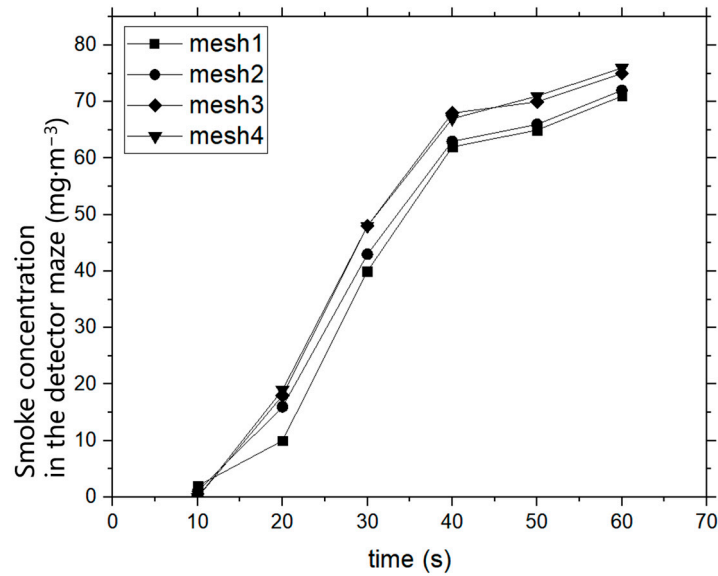


Figure 6. Grid independence verification results.

3.2. Numerical Simulation

The time–history data acquisition step was set to 0.1 s, the numerical iteration step was $\delta t = 0.1$ s, and the air flow velocity of the tuyere of the FDS simulation model was set to 0.1 m/s, 0.12 m/s, 0.14 m/s, 0.16 m/s, 0.18 m/s and 0.2 m/s. The smoke-flow mass concentration curves of the point O (the point inside the labyrinth) and point M (the point at the shell of the maze) are shown in Figure 7, which are directly outputted from the model. When the tuyere velocity is 0.1 m/s, it can be seen from Figure 7a that the mass concentration curve $d(t)$ of smoke flow at the point M outside of the cabin jumps at 9.3 s and gradually tends to oscillate, while the mass concentration curve of smoke flow at the point O in the cabin $\tilde{d}(t)$ begins to rise slowly and smoothly at 11.2 s, and finally maintains the same steady-state peak as in $d(t)$. According to the data shown in Figure 7a, $\tau_1 = \tilde{t}_0 - t_0 = 1.9$ s, and $\tau_2 = 16.5$ s were adjusted so that the calculated curve of $\tilde{d}(t)$ is in agreement with the simulated curve of Figure 8a, and the fitting error was $R = 0.9852$. When the tuyere velocity is 0.12 m/s, it can be seen from Figure 7b that the mass-concentration curve $d(t)$ of the smoke flow of M power outside of the cabin jumps at 8.4 s and gradually tends to oscillate, while the mass-concentration curve of smoke flow $\tilde{d}(t)$ of the O point smoke flow in the cabin begins to rise slowly and smoothly at 9.8 s and finally maintains

a steady-state peak of almost the same as that of $d(t)$. According to the data shown in Figure 7b, $\tau_1 = \tilde{t}_0 - t_0 = 1.4$ s and $\tau_2 = 13.6$ s were adjusted so that the calculated curve of $\tilde{d}(t)$ is consistent with the numerical simulation curve in Figure 8b, and the fitting error was $R = 0.9794$. When the tuyere velocity is 0.14 m/s, it can be seen from Figure 7c that the mass concentration curve $d(t)$ of the smoke flow of M power outside the cabin starts to jump at 7.4 s and gradually tends to oscillate, while the mass concentration curve of the smoke flow at the O point in the cabin $\tilde{d}(t)$ begins to rise slowly and smoothly at 8.6 s and finally maintains almost the same steady-state peak as $d(t)$. According to the data shown in Figure 7c, $\tau_1 = \tilde{t}_0 - t_0 = 1.2$ s, and $\tau_2 = 12$ s was adjusted so that the calculated curve of $\tilde{d}(t)$ is in agreement with the numerical simulation curve in Figure 8c, and the fitting error was $R = 0.9905$. When the tuyere velocity is 0.16 m/s, it can be seen from Figure 7d that the mass concentration curve $d(t)$ of the smoke flow of M power outside of the cabin starts to jump at 6.6 s and gradually tends to oscillate, while the mass concentration curve of the smoke flow at the O point in the cabin $\tilde{d}(t)$ begins to rise slowly and smoothly at 7.6 s and finally maintains the same steady-state peak as $d(t)$. According to the data shown in Figure 7d, $\tau_1 = \tilde{t}_0 - t_0 = 1.0$ s, and $\tau_2 = 11.5$ s was adjusted so that the calculated curve of $\tilde{d}(t)$ is in agreement with the numerical simulation curve in Figure 8d, and the fitting error was $R = 0.9919$. When the tuyere velocity is 0.18 m/s, it can be seen from Figure 7e that the mass concentration curve $d(t)$ of the smoke flow of M power outside of the cabin jumps at 6.0 s and gradually tends to oscillate, while the mass concentration curve of the smoke flow at the O point in the cabin $\tilde{d}(t)$ begins to rise slowly and smoothly at 6.9 s and finally maintains the same steady-state peak as $d(t)$. According to the data shown in Figure 7e, $\tau_1 = \tilde{t}_0 - t_0 = 0.9$ s, and $\tau_2 = 9.1$ s was adjusted so that the calculated curve of $\tilde{d}(t)$ is in agreement with the numerical simulation curve in Figure 8e, and the fitting error was $R = 0.9821$. When the tuyere velocity is 0.2 m/s, it can be seen from Figure 7f that the mass concentration curve $d(t)$ of the smoke flow of the M electricity outside of the cabin starts to jump at 5.4 s and gradually tends to oscillate, while the mass concentration curve of the smoke flow at the O point in the cabin $\tilde{d}(t)$ begins to rise slowly and smoothly at 6.3 s and finally maintains the same steady-state peak as $d(t)$. According to the data shown in Figure 7f, $\tau_1 = \tilde{t}_0 - t_0 = 0.9$ s, and $\tau_2 = 7.18$ s was adjusted so that the calculated curve of $\tilde{d}(t)$ is consistent with the numerical simulation curve in Figure 8f, and the fitting error was $R = 0.9841$.

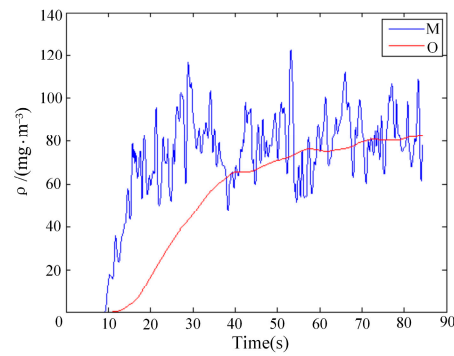
The velocity time–history curve of the smoke flow at M point outside the maze is shown in Figure 9. In Figure 9a, the effective velocity of $u(t) = \sqrt{u_x^2 + u_y^2} \approx u_x(t)$, and the mean value of the steady-state oscillation part of the time–history curve was taken to obtain $u = 0.1367$ m/s, and so far, a set of (u, τ_1, τ_2) values (0.1367, 1.9, 16.5) at the tuyere velocity = 0.1 m/s were obtained. In Figure 9b to Figure 9f, the same method was used to obtain the result that u is 0.1435 m/s, 0.1545 m/s, 0.1731 m/s, 0.1367 m/s and 0.2207 m/s, respectively, and the corresponding five sets of values are (0.1435, 1.4, 13.6), (0.1545, 1.2, 12.2), (0.1731, 1.0, 11.5), (0.2028, 0.9, 9.1) and (0.2207, 0.9, 7.18), respectively.

3.3. Parameter Fitting

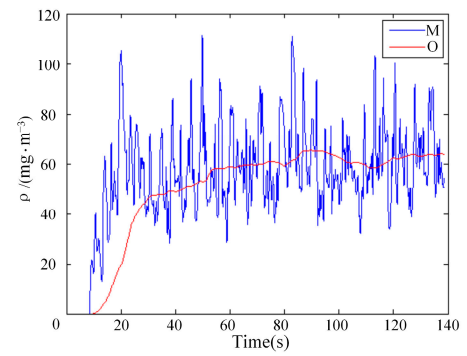
Using the same method, simulations were performed for airflow velocities of 0.12, 0.14, 0.16, 0.18 and 0.20 m/s. The simulation results are shown in Figures 7–9, and the corresponding sets of (u, τ_1, τ_2) are listed in Table 2. As the airflow velocity decreases, the time required for the $\tilde{\rho}(t)$ curve to reach a significantly stable phase gradually increases.

Table 2. Parameter calibration at airflow velocity of each tuyere.

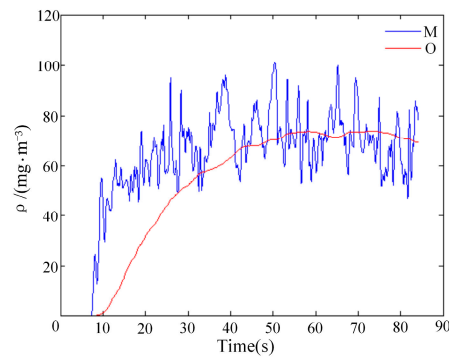
Vel. (m/s)	u (m/s)	t_0/s	\tilde{t}_0/s	τ_1/s	τ_2/s	R
0.20	0.2207	5.4	6.3	0.9	7.18	0.9841
0.18	0.2028	6	6.9	0.9	9.1	0.9821
0.16	0.1713	6.6	7.6	1.0	11.5	0.9919
0.14	0.1545	7.4	8.6	1.2	12.2	0.9905
0.12	0.1435	8.4	9.8	1.4	13.6	0.9794
0.10	0.1367	9.3	11.2	1.9	16.5	0.9852



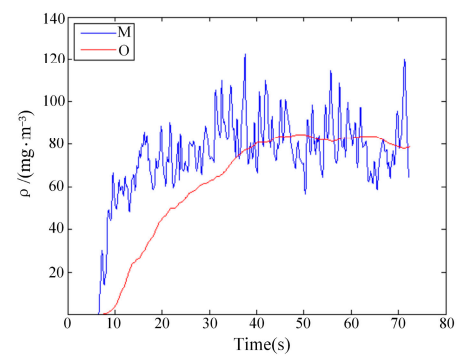
(a) 0.1 m/s



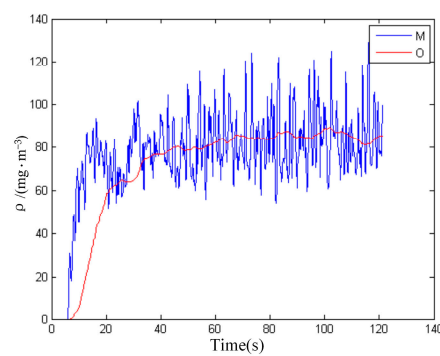
(b) 0.12 m/s



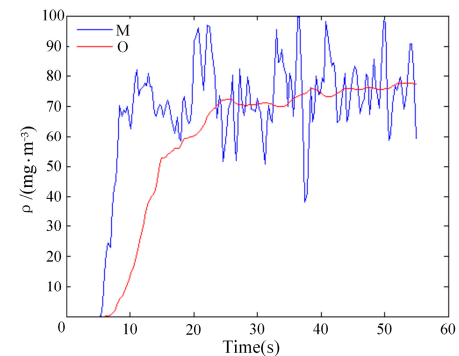
(c) 0.14 m/s



(d) 0.16 m/s



(e) 0.18 m/s



(f) 0.2 m/s

Figure 7. Smoke concentration at measuring points inside and outside of smoke labyrinth under conditions of 0.10–0.20 m/s.

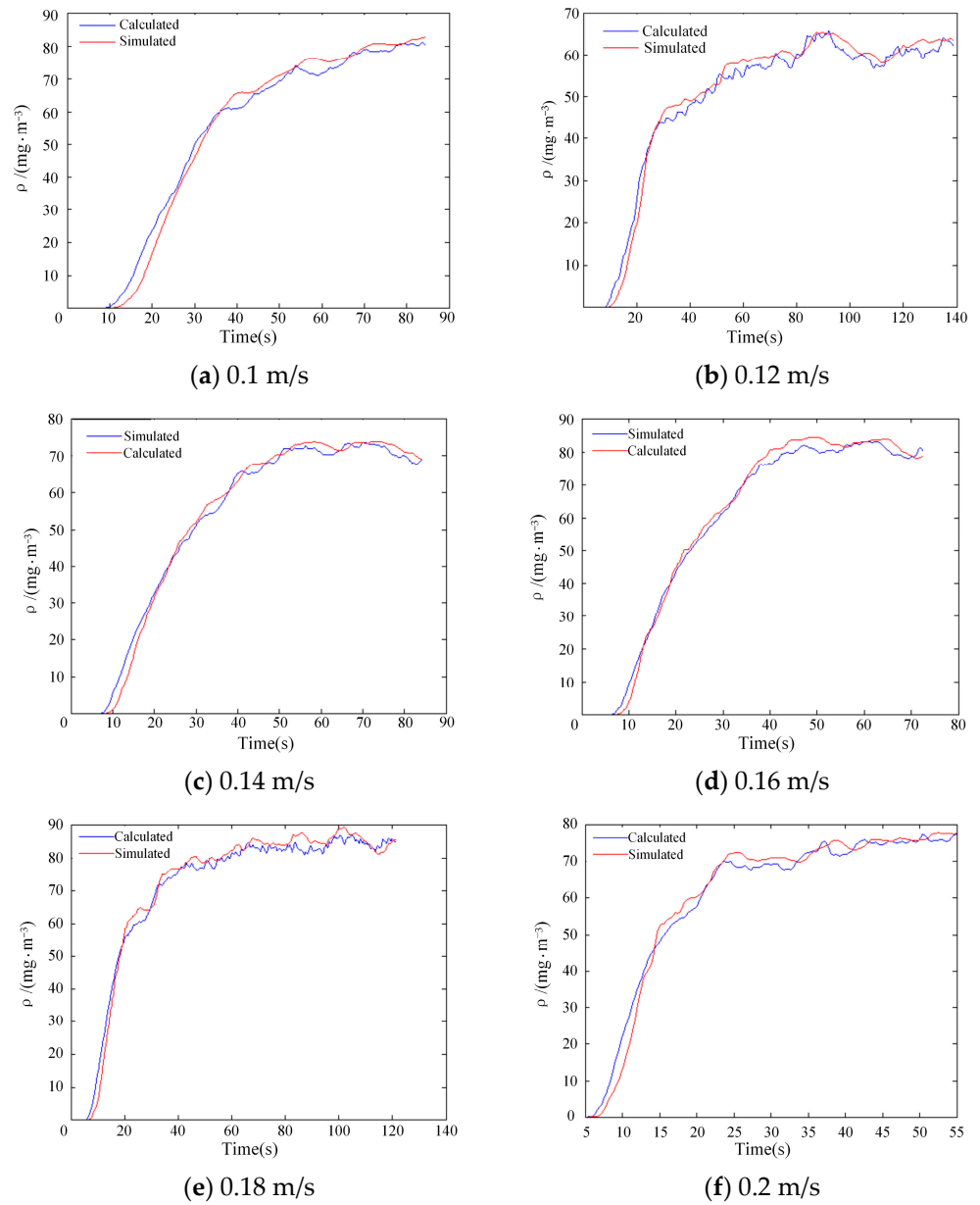


Figure 8. Fitting data of smoke labyrinth signal under conditions of 0.10–0.20 m/s.

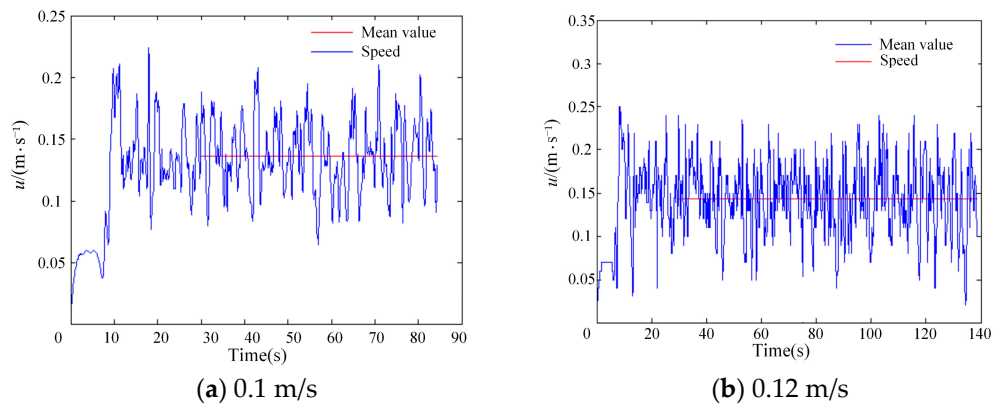


Figure 9. Cont.

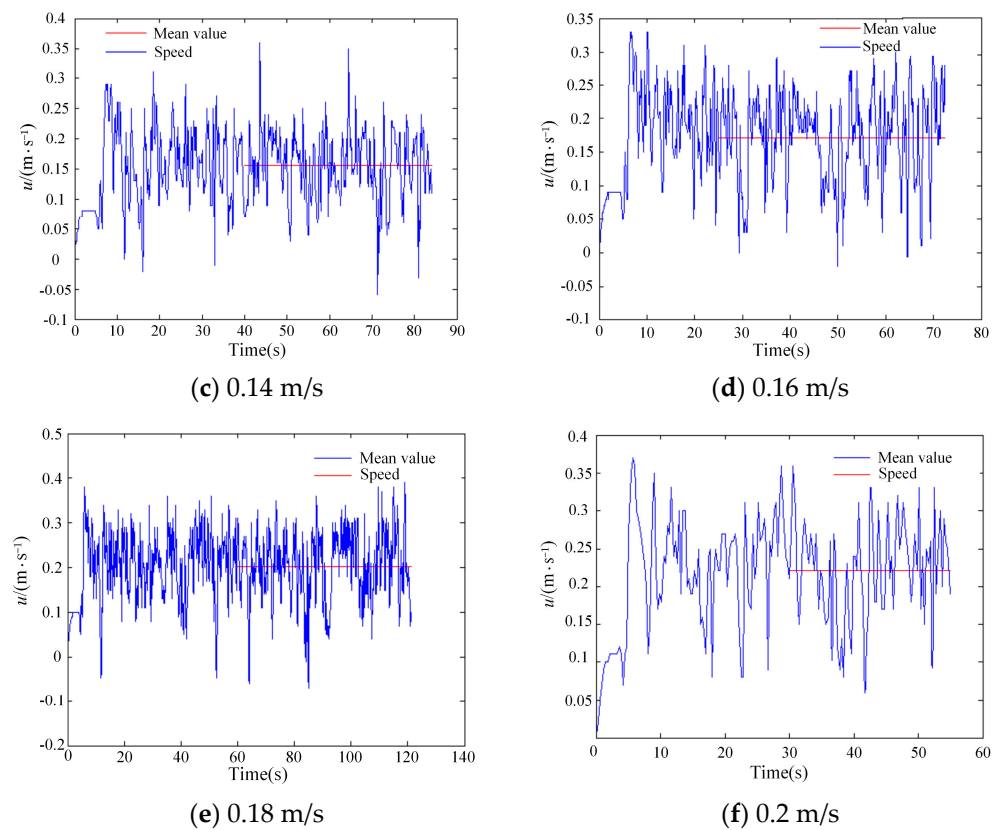


Figure 9. Time history of smoke flow velocity outside of smoke labyrinth under conditions of 0.10–0.20 m/s.

The above six sets of data (u, τ_1, τ_2) are used as the least squares fitting in the form of $\tau_1 = a_1 u^{-b_1}, \tau_2 = a_2 u^{-b_2}$, and the fitting curves are shown in Figures 10 and 11. The specific parameter expressions are as follows:

$$\tau_1 = 0.09u^{-1.43}, 0.1 \leq u \leq 0.2 \tag{6}$$

$$\tau_2 = 0.67u^{-1.59}, 0.1 \leq u \leq 0.2 \tag{7}$$

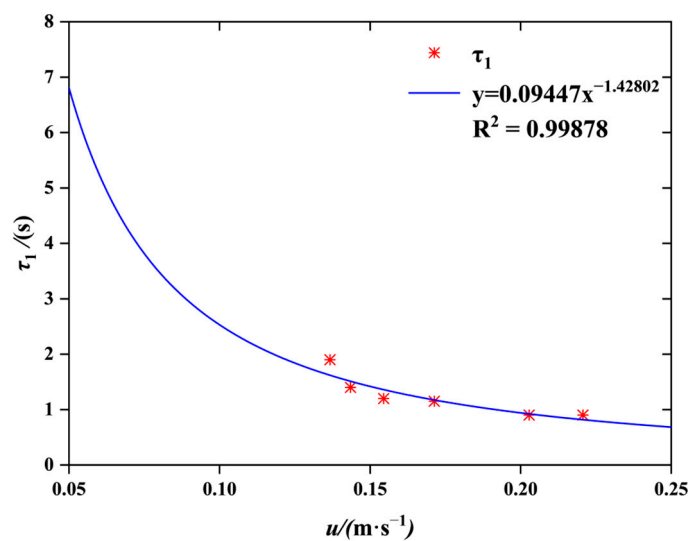


Figure 10. Results of τ_1 parameter fitting.

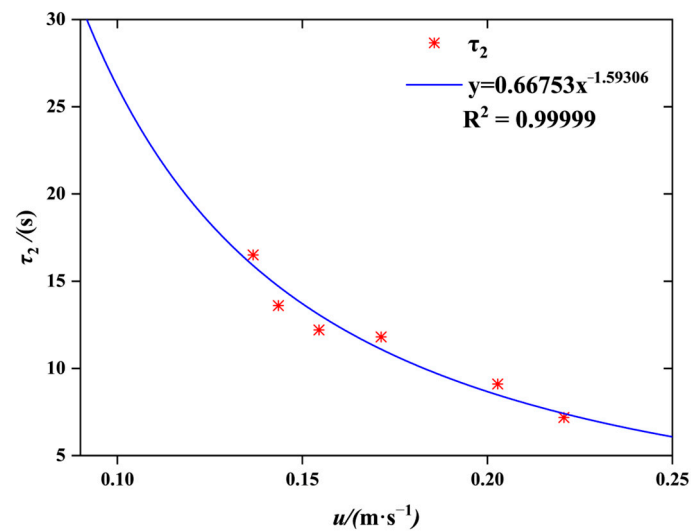


Figure 11. Results of τ_2 parameter fitting.

The Cleary hysteresis model can be used to predict the smoke response lag time of this type of smoke detector when the fire occurs, so as to determine the alarm time of the detector after the fire at different smoke flow speeds. However, considering that when the simulation model is established, although the tuyere model selects several typical working conditions of the aircraft cargo compartment, the smoke source reactant only selects the polyurethane and defines the maximum smoke–soot generation fraction and the minimum heat release rate. The smoke detector model is also specified. Therefore, it is necessary to further consider the calibration of smoke generated by different smoke sources to improve the scope of the application of these simulation conclusions. In addition, the corresponding modules can be integrated into the software through secondary development to facilitate the rapid operation of other geometric configurations of detectors on the market.

4. Experimental Verification

This experimental section was conducted in the test cargo compartment of the fire protection system laboratory at the Tianjin Aviation Electro-Mechanical Co., Ltd. cargo compartment (Tianjin, China). The cargo compartment test chamber is a multi-functional full-scale simulation test device used to simulate the potential risk of a fire inside the aircraft cargo compartment. Figure 12 shows the cargo compartment of the fire protection test laboratory, where the size is 8110 mm × 4160 mm × 1670 mm. Simulating the test cabin model, the cargo compartment is narrow at the bottom and wide at the top. Fixed smoke density sensors are installed at the front, middle and rear positions of the top of the cabin.



Figure 12. The aircraft cargo compartment ground simulation platform: the left image shows the dimensional diagram and the right image shows the actual photo.

This testing procedure was primarily broken into the following steps: (1) we installed the smoke detector in the middle position near the top of the cargo compartment test cabin,

as shown in Figure 13; (2) we installed a portable densitometer near the smoke detector to analyze the smoke concentration near the smoke detector; (3) we turned on the portable smoke density meter (Concept Smoke Systems Ltd, UK) in the cabin at the same time to collect the response signals; (4) we chose a location, arranged the smoke generator, and adjusted the smoke mode so that the smoke generated flowed at an approximately constant speed on the cabin's roof, as shown in Figure 14; (5) we recorded the smoke detector response time through video monitoring, stopped the densitometer collection, and saved the densitometer data results.



Figure 13. Layout of smoke detectors and experimental equipment in test cargo compartment.



Figure 14. Smoke movement inside cargo compartment during experiment.

Using the hysteresis model proposed in the previous section, the internal response of the smoke detector chamber can be numerically calculated based on Beer's law and the smoke density meter's response data. The prediction curve based on this numerical calculation is shown in Figure 15, which depicts the change in the refractive index of the smoke inside the smoke detector over time. The two coordinate points in the diagram represent the values at both ends of the smoke detector's alarm range, i.e., from 92% to 94%, and the corresponding alarm times are 43.1 s and 49.0 s, respectively, which is the total time from the smoke occurrence to the smoke detector reaching the alarm threshold. Setting the air leakage rate of the test airplane cargo cabin and modifying the smoke generator's smoke generation mode causes the smoke to flow at an approximately constant speed in the cabin. A total of six sets of tests at different wind speeds ranging from 0.1 m/s to 0.2 m/s were carried out. The results are shown in Table 3, where it can be seen that the alarm response of the detector becomes faster with the increase in the smoke flow speed. The alarm times of the six groups of experiments all fell within the predicted alarm range from 43.1 s to

49.0 s. Through this experiment, the accuracy of the second-order hysteresis model can be verified, which provides a positive judgment method for the design of smoke detectors.

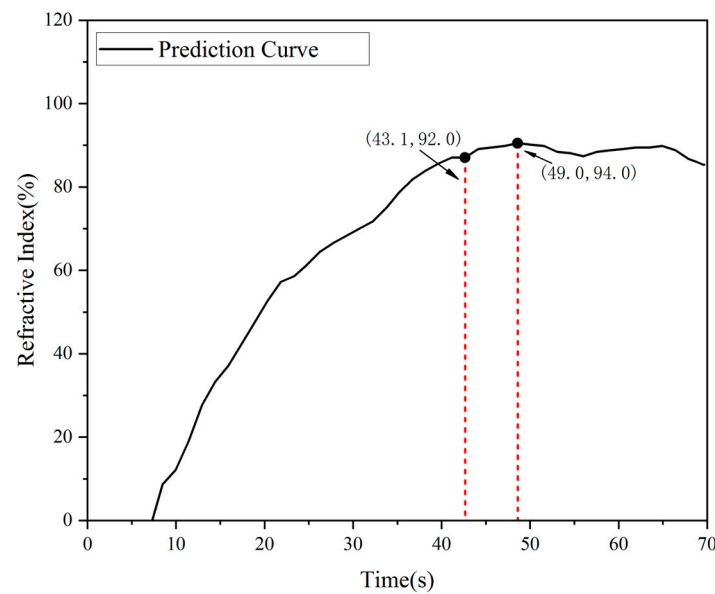


Figure 15. Response time curve of smoke detectors inside maze as predicted by parameters.

Table 3. Alarm time of aircraft cargo cabin verification experiments under different wind speeds.

Serial Number	Wind Velocity (m/s)	Cargo Tank Pressure (atm)	Air Leakage Flow Rate (m ³ /min)	Temperature (°C)	Alarm Time (s)
1	0.10	1.01	1.26	25.1	48.9
2	0.12	1.00	1.33	25.0	48.4
3	0.14	1.02	1.41	25.2	45.1
4	0.16	0.98	1.48	24.9	45.5
5	0.18	0.98	1.54	24.8	44.4
6	0.20	1.01	1.60	24.9	43.1

5. Conclusions

In this paper, the hysteresis effect of photoelectric smoke detectors was investigated, and the calibration methods of the smoke velocity u , retention time τ_1 and mixing time τ_2 were determined through the analysis of Cleary’s two-stage model. A smoke detector model and a numerical simulation wind tunnel were constructed in FDS to explore the detector response parameters at six ambient wind speeds ranging from 0.1 m/s to 0.2 m/s. A two-stage hysteresis model for evaluating the different ambient wind speeds was obtained by fitting the parameters, where $\tau_1 = 0.09u^{-1.43}$ and $\tau_2 = 0.67u^{-1.59}$. Finally, a full-size physical cargo hold experiment was performed for the prediction model, and the anticipated alert range is from 43.1 s to 49.0 s, with the actual alarm times falling within the range, confirming the model’s accuracy. Cleary’s two-stage hysteresis model can be extended and applied to the design of a fire prevention system for an airplane’s cargo hold, as well as to guide the structural design and layout of smoke detectors, particularly on a large aircraft.

Author Contributions: Software, S.W.; Writing—original draft, H.C.; Writing—review & editing, C.R. and S.L.; Visualization, M.W.; Project administration, H.Z. All authors have read and agreed to the published version of the manuscript.

Funding: This study was supported by the National Natural Science Foundation of China (No. U2133201), the National Key R&D Program of China (No. 2023YFC3010203-5), and the Civil Aircraft Scientific Research Project of the Ministry of Industry and Information Technology (BB2320000048).

Institutional Review Board Statement: Not applicable.

Informed Consent Statement: Not applicable.

Data Availability Statement: The original contributions presented in the study are included in the article, and further inquiries can be directed to the corresponding author.

Conflicts of Interest: Authors Hongwei Cui, Shengdong Wang, and Minqiang Wang were employed by the company Tianjin Aviation Electro-Mechanical Co., Ltd. The remaining authors declare that the research was conducted in the absence of any commercial or financial relationships that could be construed as a potential conflict of interest.

References

1. HB7098-1994; Aviation Industry Standards of the People's Republic of China. China Aviation Industry Corporation 301 Research Institute: Beijing, China, 1994.
2. Han, L.; Lin, G.; Fang, J.; Wang, J.; Zhang, Y. Effect of optical labyrinth on the response performance of aircraft cargo hold smoke detectors. *Fire Sci.* **2016**, *25*, 208–212.
3. Wang, J.; Lu, K.; Lu, S.; Zhang, H. Experimental study on ceiling temperature profile of sidewall fires at reduced pressure in an aircraft cargo compartment. *Exp. Therm. Fluid Sci.* **2017**, *82*, 326–332. [[CrossRef](#)]
4. Li, C.; Xu, W.; Jin, Y.; Wang, C.; Liu, Q.; Zhang, H. Numerical investigations on combustion characteristics of full-size cabin fire with typical material pyrolysis and burnout under different fire source positions. *Case Stud. Therm. Eng.* **2024**, *54*, 104075. [[CrossRef](#)]
5. Keller, A.; Loepfe, M.; Nebiker, P.; Pleisch, R.; Burtscher, H. On-line determination of the optical properties of particles produced by test fires. *Fire Saf. J.* **2006**, *41*, 266–273. [[CrossRef](#)]
6. Kruell, W.; Schultze, T.; Willms, I.; Freiling, A. Developments in non-fire sensitivity testing of optical smoke detectors-proposal for a new test method. *Fire Saf. Sci.* **2011**, *10*, 543–554. [[CrossRef](#)]
7. Zhou, Y.; Shi, L.; Li, C.; Zhang, H.; Zheng, R. Scattering Characteristics of Fire Smoke and Dust Aerosol in Aircraft Cargo Compartment. *Fire Technol.* **2023**, *59*, 2543–2565. [[CrossRef](#)]
8. Zheng, R.; Lu, S.; Shi, Z.; Li, C.; Jia, H.; Wang, S. Research on the aerosol identification method for the fire smoke detection in aircraft cargo compartment. *Fire Saf. J.* **2022**, *130*, 103574. [[CrossRef](#)]
9. Chen, X.; Shao, Z.; Yang, J. Comparison between actual and simulated smoke for smoke detection certification in aircraft cargo compartments using the CFD method. *Fire Technol.* **2020**, *56*, 469–488. [[CrossRef](#)]
10. Chen, X.; Yan, X.; Yang, J. Closed-Loop Control Strategy for Simulated Smoke Concentration in Aircraft Cargo Compartment Mock-Up. *Fire Technol.* **2023**, *59*, 2263–2297. [[CrossRef](#)]
11. Papa, R.; Andrade, C.R.; Zapparoli, E.L.; de C. Santos, L.C. CFD analysis of smoke transport inside an aircraft cargo compartment. *J. Braz. Soc. Mech. Sci. Eng.* **2016**, *38*, 327–334. [[CrossRef](#)]
12. Blake, D.; Suo-Anttila, J. Aircraft cargo compartment fire detection and smoke transport modeling. *Fire Saf. J.* **2008**, *43*, 576–582. [[CrossRef](#)]
13. Oztekin, E.S.; Blake, D.; Lyon, R.E. Fire induced flow behavior in a ventilated aircraft cargo compartment. In Proceedings of the 13th International Conference and Exhibition on Fire and Materials, San Francisco, CA, USA, 28–30 January 2013; pp. 28–30.
14. Oztekin, E.S. Heat and mass transfer due to a small-fire in an aircraft cargo compartment. *Int. J. Heat Mass Transf.* **2014**, *73*, 562–573. [[CrossRef](#)]
15. Suo-Anttila, J.; Gill, W.; Luketa-Hanlin, A.; Gallegos, C. *Cargo Compartment Smoke Transport Computational Fluid Dynamic Code Validation*; US Department of Transportation, Federal Aviation Administration: Washington, DC, USA, 2007.
16. Lu, K.H.; Mao, S.H.; Wang, J.; Lu, S. Numerical simulation of the ventilation effect on fire characteristics and detections in an aircraft cargo compartment. *Appl. Therm. Eng.* **2017**, *124*, 1441–1446. [[CrossRef](#)]
17. Zhang, P.; Meng, M.; Wang, J. Optimised arrangement technology and platform development for aircraft cargo hold smoke detection system. *Fire Sci.* **2016**, *25*, 228–232.
18. Heskestad, G. Generalized characterization of smoke entry and response for products of combustion detectors. In *Proceeding of the Fire Detection for Life Safety Symposium, Washington, DC, USA, 31 March–1 April 1975*; National Academy of Science: Washington, DC, USA, 1977; pp. 93–127.
19. Brozovsky, E.L. A first approximation method for smoke detector placement based on design fire size, critical velocity, and detector aerosol entry lag time. *Fire Technol. Fourth Quart.* **1995**, *31*, 336–353. [[CrossRef](#)]

20. *UL217*; Standard for Safety for Single and Multiple Station Smoke Alarms. Underwriters Laboratories Inc.: Northbrook, IL, USA, 2006.
21. Cleary, T.; Chernovsky, A.; Grosshandler, W.L.; Anderson, M.D. Particulate entry lags in spot-type smoke detectors. In Proceeding of the 6th International Symposium of IAFSS Poitiers, Poitiers, France, 5–9 July 1999; pp. 779–790.

Disclaimer/Publisher’s Note: The statements, opinions and data contained in all publications are solely those of the individual author(s) and contributor(s) and not of MDPI and/or the editor(s). MDPI and/or the editor(s) disclaim responsibility for any injury to people or property resulting from any ideas, methods, instructions or products referred to in the content.